euspen's Special Interest Conference Meeting:
Advancing Precision in Additive Manufacturing
www.euspen.eu

Improving the inflow and outflow of Triply Periodic Minimal Surfaces for additively manufactured heat exchangers

Eckart Uhlmann[1,2], Julian Polte[1,2], Janek Fasselt[1], Christoph Lübbert[1]

[1]*Fraunhofer Institute for Production Systems and Design Technology IPK, Germany*
[2]*Institute for Machine Tools and Factory Management IWF, Technische Universität Berlin, Germany*

janek.fasselt@ipk.fraunhofer.de

Abstract

Heat exchangers are critical components in various industrial applications, enabling energy transfer between different media, typically liquids or gases. Traditional manufacturing methods, such as rolling and welding, limit the complexity of the heat transfer structures and require extensive assembly. Additive Manufacturing presents a promising alternative, offering the potential to produce highly intricate internal structures with greater design flexibility, particularly Triply Periodic Minimal Surfaces. These structures can only be produced via Additive Manufacturing, enhancing the surface area available for heat transfer while reducing pressure loss in the heat exchanger, resulting in significantly improved energy efficiency. However, effectively controlling fluid flow into and out of these structures remains a significant challenge. This study employs a parametric modelling approach to optimize the inflow and outflow design geometry, achieving a 26.2 % reduction in pressure loss in tested specimens.

Additive Manufacturing, Triply Periodic Minimal Surfaces, Simulation

1. Introduction

Heat transfer $\dot{Q}$ between media is a fundamental process across diverse technological landscapes, including the chemical industry, combustion engines, and thermodynamic cycles in modern heat pumps. Heat exchangers enable efficient heat transfer $\dot{Q}$ with or without mixing the utilized substances, while minimizing pressure loss Δp_V . Traditionally, heat exchangers are made from rolled and welded sheets or tubes, which restricts geometric optimization for specific applications, resulting in a higher pressure loss Δp_V and leakage risks. In contrast, Additive Manufacturing (AM) allows the production of intricate structures in monolithic parts that cannot be achieved using conventional manufacturing methods. Triply Periodic Minimal Surfaces (TPMS) have emerged as particularly advantageous due to their ability to enhance heat transfer efficiency $\eta_{\dot{Q}}$ by maximizing the surface-to-volume ratio [1]. These surface-based lattices can be defined by mathematical function.

Despite their benefits, controlling fluid dynamics on the borders of these intricate TPMS structures poses significant challenges. Current designs often feature flat walls at the inflow and outflow geometry, which contributes to a substantial pressure loss Δp_V. A recent study highlights the importance of optimizing flow channel geometries to enhance performance [2].

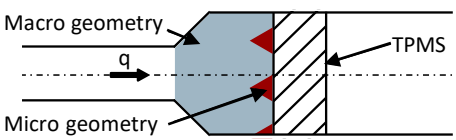

Figure 1. Distinction between micro and macro geometry at the entry zone into a TPMS structure.

The first step involves classifying the space under consideration by distinguishing between micro and macro geometry. A pipe flow directed into a component with an internal TPMS structure, accompanied by a change in flow cross-section is illustrated in Figure 1. In this scenario, the macro-geometry can be modified, for example, by using baffles or a specially adapted TPMS structure [3]. Alternatively, the area can be left free, allowing for adaptations to the microgeometry, in this case the shape of the TPMS directly at the inflow. This paper focuses on the latter case.

To optimize the inflow and outflow geometry of TPMS structures at the micro level, specifically the flow channel closure (FCC), two different approaches can be employed.

1. The TPMS structure is modified integrally. This can be done by first creating the structure and then modifying it using CAD tools, or by altering the function directly.
2. The TPMS structure remains unchanged and additional geometries are created that connect to the TPMS.

LEE ET AL. adopted the first approach, utilizing special filter functions to alter the local geometric shape of TPMS [2]. They extended the function describing the isosurface of a TPMS with sigmoid functions, enabling manipulation of the mathematical equation only at the beginning and end of a series of unit cells. By varying the parameters of the level equation, a TPMS domain can be locally closed, achieving a simulated reduction in pressure loss $\Delta p_{V,S}$ of 20 %. A significant limitation of this method is, that the geometric shape of the closure is constrained. Both the inflow and outflow geometry are closed similarly, which cannot be further optimized in terms of flow dynamics.

To date, no literature exists for the second variant. The advantage of this approach is that the geometric shape of the inflow and outflow geometry can be freely selected, as they are independent of the mathematical definition of the TPMS. This method can also be applied to structures for which no mathematical function exists.

This paper aims to develop a solution for optimizing the inflow and outflow geometry of TPMS structures and to validate their

effectiveness through computational simulations and experimental testing. Subsequent sections will detail the methodology for optimizing these geometries, present the results of simulations and experiments, and discuss the implications of the findings for the design of efficient heat exchangers.

2. Methods

Drop-shaped streamlined bodies exhibit low drag coefficients c_W, making them suitable for the FCC design. In this context, flow is directed through one or more TPMS cells, entering from one side and exiting from the other, as illustrated in Figure 2. The concept involves dividing a streamlined body at its widest point and using each half to close the flow channel. To ensure geometric continuity G, transition areas (highlighted in grey) are constructed between the streamlined body and the TPMS.

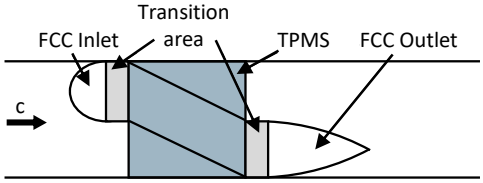

Figure 2. Basic concept for designing a TPMS with geometrically optimised entry and exit areas.

There are many different design approaches for streamlined bodies. KÜMMEL [4] recommends the four-digit profiles of the NACA profile system. This collection of defined two-dimensional airfoils also includes those that are axially symmetrical and therefore have a teardrop shape. Key geometric parameters include the diameter d_{max}, the distance from the circle's centre to the profile's leading edge length l_d, and the total length l, as illustrated in Figure 3.

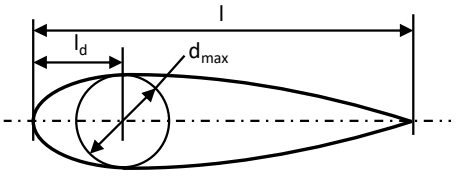

Figure 3. Design of a streamlined body (illustration modified according to [4]).

For the NACA profile the leading edge length l_d is one third of the total length l. The main variation is achieved by Equation 1, where the diameter d_{max} is defined by the TPMS channel width, resulting in a total length l dependent on ε_P.

$$\varepsilon_P = \frac{d_{max}}{l} \qquad (1)$$

2.1. Modelling of the inflow and outflow

Figure 4 shows the main sub steps for modelling the FCC at the inflow. In order to achieve a constant termination of the FCC at the edge of the unit cell, a 3 x 3 grid is initialized, extending beyond the boundaries of the unit cell. The edges at which the FCCs are to be connected are then extracted (Figure 4a). The three-dimensional problem is projected onto two-dimensional, equidistant planes. Two cutting planes intersect with the TPMS surface, producing so called curvature curves that fulfil the G2 continuity criterion (Figure 4b/c). This collection of curves defines the contour of the FCC, which is then used to generate a three-dimensional surface that integrates seamlessly with the TPMS cell (Figure 4d).

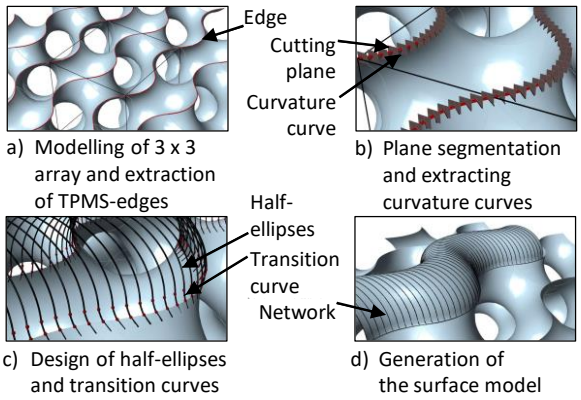

Figure 4. Sub steps for modelling of the FCC.

The FCC is duplicated and moved to cover the second open channel, then trimmed to the unit cell outline. The same process is applied to the FCC on the opposite side. The FCC's shape is defined during curve design: for the inlet-side FCC, an elliptical shape approximates the streamline profile. Transition zones ensure smooth connection to the TPMS with G2 continuity. Figure 5 illustrates FCC contour design. Half ellipses are defined by base points and the ellipse length l_{El}. Transition areas, formed by connecting curves, link TPMS support points to base points, maintaining G2 continuity.

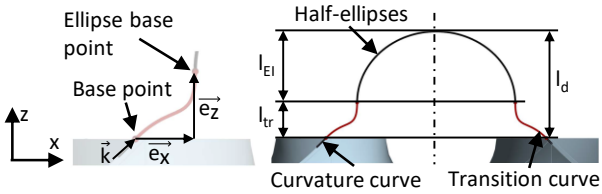

Figure 5. Design of contours for the FCC.

The ellipse base point is created by shifting the base point by the vector $\vec{e}$. The vector $\vec{k}$ can be generated using the end points of the curvature curves. This is normalised and then its x-component is extracted, which is then multiplied by the factor b_{tr} to give the x-component of vector $\vec{e}$. The z-component of vector $\vec{e}$ is the constant transition length l_{tr}. This is obtained by subtracting the leading edge length l_d from ellipse length l_{El}. In the following, FCCs used are scaled based on these parameters, with values adjusted relative to side length e of a unit cell to maintain consistent shape

2.2. Experimental setup

Investigations of the optimized FCC for the heat exchanger are conducted under specific boundary conditions. Water is selected as working fluid for the experiments due to its incompressibility, which also simplifies simulations. Additionally, the higher density of water ρ_w allows for a more significant pressure loss Δp_V, enhancing the visibility of the effects being studied. Six test specimens are utilized to assess the effectiveness of the FCC, categorized as either "optimized" (equipped with FCC) or "flat," (no changes made) as detailed in Table 1.

Table 1 Overview geometric parameters of test samples

Sample	Inflow	Outflow	Lattice dimension
1	optimized	optimized	1 x 1
2	flat	optimized	1 x 1
3	optimized	flat	1 x 1
4	flat	flat	1 x 1

This fluid mechanical investigation is performed using only one fluid (water). A flow is generated that impinges on one solid domain and flows through the other domain. The testing employs a circular cross-section for the sample bodies to avoid any potential effects from changes in cross-sectional shape at the transition between the pipe and the samples. Each specimen features at least one complete TPMS unit cell within the pipe flow. The internal diameter d_i of the pipe flow is critical for determining the characteristic length l_c, with $l_c = d_i$. To maximize pressure loss differences between samples, the flow velocity q must be as high as feasible. For a given volume flow $\dot{V}$, this can be achieved by reducing the internal diameter d_i and thus the cross-sectional area A_V according to Equation 2.

$$q = \frac{\dot{V}}{A_V} = \frac{4 \cdot \dot{V}}{\pi \cdot d_i^2} \quad (2)$$

The outlet should be a high-temperature (HT) tube into which the test specimens can be inserted. The outer diameter d_a matches the standard dimensions of HT pipes. To achieve meaningful measurement results, the macro-geometry of the TPMS structures must clearly dominate over the surface structure resulting from AM. The smallest reasonable side length of unit cells is therefore set to e = 5 mm, leading to a minimum inner diameter $d_{i.,min}$ = 28 mm.

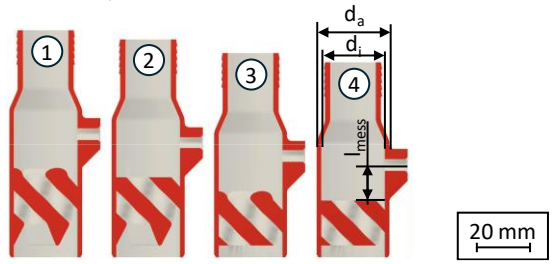

Figure 6. Test specimens 1 to 4 in half section.

The fluid inflow is vertically through the top, the hole on the side is provided so a pressure gauge can be attached for measurement (see Figure 6). The different total lengths l_{Prob} result from the fact that the same distance to the pressure measuring point l_{mess} = 20 mm and to the flow outlet is provided before and after the TPMS geometry for each sample body. This creates comparable conditions. The experimental setup is schematically outlined in Figure 7.

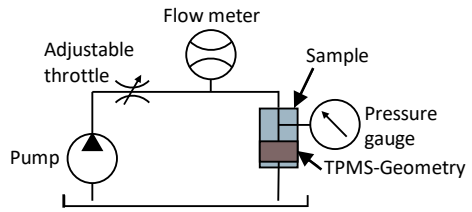

Figure 7. Experimental setup to measure the pressure loss $\Delta p_{V,E}$.

2.3. Simulation

The fluid simulation process for the TPMS consists of several systematic steps, illustrated in Figure 8.

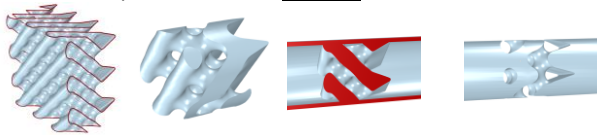

a) Area b) Solid body c) Flow tube d) Fluid domain

Figure 8. Sub steps for generating the fluid domain for the simulation.

First, the surface geometry delineating the two fluid domains is modelled (Figure 8a). In this study, one fluid domain is considered while the opposing domain is represented as a solid. Next, a cylindrical shape with a diameter d_i of the flow tube is centred in the surface geometry (Figure 8b). A connecting tube is then added to establish a continuous flow path (Figure 8c), with an upstream and downstream length of l_{tube} = 100 mm to adequately capture flow dynamics around the TPMS geometry. Finally, the fluid domain is extracted by creating a negative space, resulting in 3D model data for the flow area, with inflow and outflow geometry predefined.

The simulation process begins with the definition of all boundary conditions and parameters. Five volume flows $\dot{V}_S$ are established for comparison with experimental results, spanning between 15 L/min ≤ $\dot{V}_S$ ≤ 170 L/min. To assess flow behaviour, the Reynolds number $Re_{s,min}$ = 11,346 is calculated, indicating turbulent flow conditions, as it exceeds the critical value Re_{crit} = 2,300 [5]. Consequently, the k-omega turbulence model is employed to approximate the turbulent influences on the flow state. The simulation is based on the numerical solution of the Reynolds-Averaged Navier-Stokes (RANS) equations, with the quality of results assessed through residuals r.

3. Results and discussion

In the following, the results from the simulations and experiments are presented and discussed. It was found that the optimisations at the inflow and outflow geometries result in a significantly lower pressure loss Δp_V.

3.1. Simulation

The simulation results are first analysed qualitatively and then graphically. To determine the pressure loss $\Delta p_{V,S}$, the inlet-area-weighted average static pressure $p_{stat,in}$ is determined at the inlet of the flow tube. The outlet-area-weighted average static pressure is $p_{stat,out}$ = 0 Pa. Due to mass flow conservation, the flow velocity q_S and subsequently the dynamic pressure p_{dyn} at the inlet and outlet are the same. The pressure loss caused by the TPMS structure $\Delta p_{V,S}$ is therefore equal to the static pressure $\Delta p_{V,S} = p_{stat,in}$ at the inlet. Figure 9 shows the simulation results for specimens 1 to 4 with a quadratic relationship between the static pressure p_{stat} and the volume flow $\dot{V}_S$.

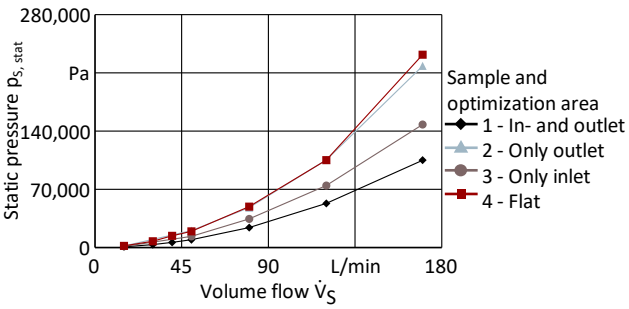

Figure 9. Results of CFD simulations of samples 1 to 4.

The optimized FCC can achieve a significant reduction in the pressure loss $\Delta p_{V,S}$. The efficiency η_{opt} of this improvement can be described using Equation 3. The value indicates the percentage by which the pressure loss of the optimized geometry $\Delta p_{V,opt}$ is lower than the pressure loss of the flat geometry $\Delta p_{V,flat}$.

$$\eta_{opt} = \left(1 - \frac{\Delta p_{V,opt}}{\Delta p_{V,flat}}\right) \quad (3)$$

The arithmetic mean of the efficiency η can be calculated across all volume flows $\dot{V}_S$. This is suitable for quantifying the influence of the optimizations. By using both optimized FCCs, a reduction of the TPMS structure pressure loss $\Delta p_{V,S}$ by the efficiency $\eta_{S,in+out}$ = 52.9 % is achieved in the simulated value range. If only one optimized geometry is used in each case, $\eta_{S,in}$ = 30.9 % and $\eta_{S,out}$ = 1.6 % are achieved.

Figure 10 shows samples 1 and 4 to compare the optimized with the flat geometry. At the inflow, it can be clearly seen how the vertical wall leads to a strong separation and thus a turbulent vortex zone directly behind the inflow. This effect is significantly less pronounced with the optimized elliptical geometry. On the outflow, it can be seen that the turbulent vortex zones decrease more quickly with the optimized geometry.

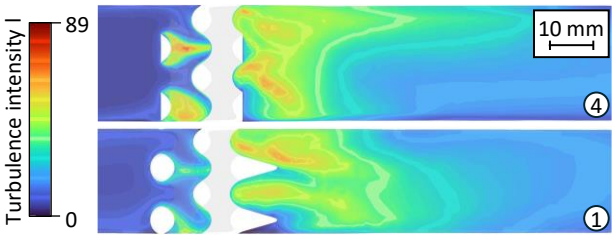

Figure 10. Turbulence intensity I of samples 1 and 4. The medium is water at a temperature $\vartheta_W = 20$ °C and a volume flow rate $\dot{V} = 40$ L/min.

3.2. Experiment

The results of the series of measurements are shown in Figure 11.

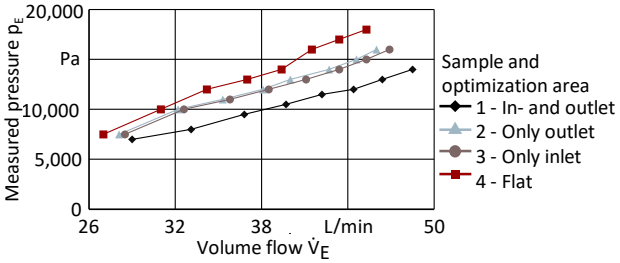

Figure 11. Results of the experimental investigation of samples 1 to 4.

The volume flow $\dot{V}_E$ depends on the pressure loss $\Delta p_{V,E}$, causing variations in x-axis measuring points between test specimens. To enable comparison at identical flow velocities q_E and minimize measurement error, a quadratic regression is applied to each measurement series with a significance level of $\alpha_{Reg} = 0.01$. The pressure loss Δp_V is quadratically dependent on flow velocity q [6], making quadratic regression the appropriate method. The results, shown in Table 2, indicate that all p-values are below the significance level of $\alpha_{Reg} = 0.01$, confirming statistical significance. The regression models effectively describe the relationship between volume flow $\dot{V}_E$ and the measured pressures Δp_E.

Table 2 Experimental results based on quadratic regression

Sample	p-value	$\Delta p_{\dot{V}=40L/min}$	$\xi_{Re=15,000}$	$\bar{\eta}_E$
4 flat	$8{,}20 \cdot 10^{-8}$	14 833 Pa	32,2	-
3 opt. inflow	$1{,}43 \cdot 10^{-7}$	12 940 Pa	30,6	9,9 %
2 opt. outflow	$1{,}60 \cdot 10^{-6}$	12 666 Pa	29,5	11,4 %
1 opt. In- & Outflow	$1{,}38 \cdot 10^{-6}$	10 798 Pa	25,2	26,2 %

The values given in the table are predictions of the regression models that lie within the value range $\dot{V}_E$ of the measured values. The third column shows the pressure loss $\Delta p_{\dot{V}=40L/min}$ for a volume flow $\dot{V} = 40$ L/min. This is followed by the pressure loss coefficients $\zeta_{Re} = 15{,}000$ for the Reynolds number Re = 15,000. Finally, the efficiencies η_E are listed as an arithmetic mean over the measuring range $\dot{V}_E$.

4. Conclusion

Both in the simulation and in the experimental investigation, the pressure loss Δp_V was significantly reduced by the optimized inflow and outflow geometries. Figure 12 shows the efficiency η_{opt} for the geometry optimized on both sides (specimen 1) compared to the flat geometry (specimen 4). The efficiency $\eta_{S,opt}$ from the simulation remains almost constant over the volume flow $\dot{V}$, while the efficiency $\eta_{E,opt}$ from the experimental investigation increases with the volume flow $\dot{V}$. However, $\eta_{E,opt}$ is generally lower than $\eta_{S,opt}$, indicating that some external influences were not considered in the simulation, such as additional pressure losses Δp_V at transitions and different surface qualities.

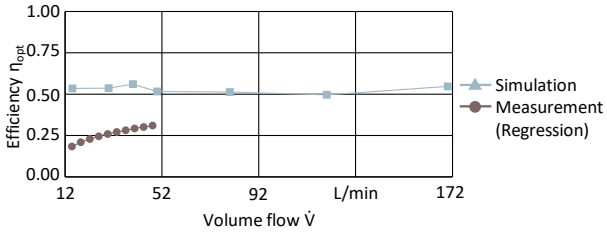

Figure 12. Comparison of efficiency η_{opt} from simulation and experiment.

The proportional influence of the inflow and outflow geometry can be compared using samples 2 and 3, each with one FCC. Significant differences exist between simulation and experimental results. Test results show that the efficiencies of the inflow optimization $\eta_{E,in} = 9.9$ % and outflow optimization $\eta_{E,out} = 11.4$ % approximately add to a combined efficiency of $\eta_{E,in+out} = 26.2$ % (Table 2). In contrast, the simulated efficiencies $\eta_{S,in} = 30.9$ % and $\eta_{S,out} = 1.6$ % are substantially lower than the combined efficiency of sample 1 with both optimizations $\eta_{S,in+out} = 52.9$ %. This discrepancy may be due to an overestimation of turbulence at the flat wall in the simulation. The relatively higher $\eta_{S,in}$ proportion suggests excessive turbulence influence, which could explain the low efficiency $\eta_{S,out}$ for the outflow-side optimized sample. The improvement in $\eta_{S,in+out}$ compared to $\eta_{S,in}$ indicates that the optimized inflow geometry mitigates this overestimated turbulence, allowing for a measurable effect from the optimized outflow geometry. Future simulations should consider samples with multiple unit cells in the flow direction to reduce mutual influence by increasing the distance between the inlet and outlet. The developed parametric modelling approach for the optimisation of the inflow and outflow geometries will significantly improve the overall efficiency of TPMS based heat exchangers.

References

[1] Feng J, Fu J, Yao X, and He Y 2022 Triply periodic minimal surface (TPMS) porous structures: from multi-scale design, precise additive manufacturing to multidisciplinary applications *Int. J. Extrem. Manuf.* **4** 022001 doi:10.1088/2631-7990/ac5be6

[2] Lee J-W, Oh S-H, Jeon E, Kim J, and Park K 2022 Functional gradation of the morphological properties of TPMS channel for enhanced flow performance *Materials & Design* **224** 111413

[3] Jiang Y, Hu J, Wang S, Lei N, Luo Z, and Liu L 2023 Meshless Optimization of Triply Periodic Minimal Surface Based Two-Fluid Heat Exchanger *Computer-Aided Design* **162** 103554

[4] Kümmel W 2004 Technische Strömungsmechanik (Wiesbaden: Vieweg+Teubner)

[5] Oertel H, Böhle M and Dohrmann U 2006 Strömungsmechanik: Grundlagen, Grundgleichungen, Lösungsmethoden, Software-beispiele 4., Studium Technik (Wiesbaden: Vieweg)

[6] Sigloch H 2022 Technische Fluidmechanik Berlin, (Heidelberg: Springer)